Journal of Applied Mechanics Vol.9, pp.1077-1084 (August 2006)

JSCE

Macro and Microscopic Bonding Fracture Mechanism Along FRP-concrete Bond Interface

FRP - コンクリート接着界面の剥離破壊メカニズムに関するマクロ・マイクロ的検討

Zhishen WU * and Jun YIN **
呉 智深・殷 峻

* Member Dr. of Eng. Prof. Dept. Urban & Civil Eng. Ibaraki University
(4-12-1, Nakanarusawa-cho, Hitachi-shi, Ibaraki 316-8511)
** Member Dr. of Eng. Advanced Simulation Technology of Mechanics (ASTOM)
(RIKEN 2-1,Hirosawa, Wako-shi, Saitama 351-0198)

The strengthening performance of fiber reinforced polymers (FRP) to concrete structures may be significantly limited due to the interfacial debonding failure along the FRP-concrete bond interface. Experimental work shows such a debonding fracture, in most cases, occurs through the interfacial concrete adjacent to bond interface. Although the interfacial debonding along FRP-concrete interface macroscopically represents a shear-dominated fracture that resembles mode II fracture, the crack in interfacial concrete is generally considered to initiate in mode I fracture followed by the aggregate interlock along the crack surface. This paper emphasizes the discussion of interfacial fracture that occurs in concrete from the viewpoint of fracture energy of concrete. To investigate such a debonding mechanism due to mode I fracture of concrete, both conventional smeared crack models and a displacement discontinuity model are used to simulate the fracturing process. A finite element analysis based on both assumptions of mode II fracture along FRP-concrete interface and mode I fracture within interfacial concrete layer is performed, and the results are compared among the different assumptions. The effects of concrete behavior of both tensile and shear fracture energies on load-carrying capacity bond interface are discussed qualitatively.

Key Words: *Interfacial debonding, mode II fracture, mode I fracture, smeared crack model, fracture energy*

1. Introduction

The strengthening performance of fiber reinforced polymers (FRP) to concrete structures may be significantly limited due to the interfacial debonding failure along the FRP-concrete bond interface. Experimental work shows such a debonding fracture, in most cases, occurs through the interfacial concrete adjacent to bond interface. Although the interfacial debonding along FRP-concrete interface macroscopically represents a shear-dominated fracture that resembles mode II fracture, the crack in interfacial concrete is generally considered to initiate in mode I fracture followed by the aggregate interlock along the crack surface. This paper emphasizes the discussion of interfacial fracture that occurs in concrete from the viewpoint of fracture energy of concrete. To investigate such a debonding mechanism due to mode I fracture of concrete, both conventional smeared crack models and a displacement discontinuity model are used to simulate the fracturing process. A finite element analysis based on both assumptions of mode II fracture along FRP-concrete interface and mode I fracture within interfacial concrete layer is performed, and the results are compared among the different assumptions. The effects of concrete behavior of both tensile and shear fracture energies on load-carrying capacity bond interface are discussed qualitatively.

Describing crack propagation in concrete, the conventional rotating and fixed smeared crack models are primary approaches, which have been implemented in quite a few commerial FE codes. Both models treat the concrete crack as mode I fracture by employing mode I fracture energy G_f^I. Another method is a displacement discontinuity model that was orignally developed for capturing strong discontinuity in brittle materials and dealed with only mode I fracture normal to the crack surface. In a modified version, the mode II fracture

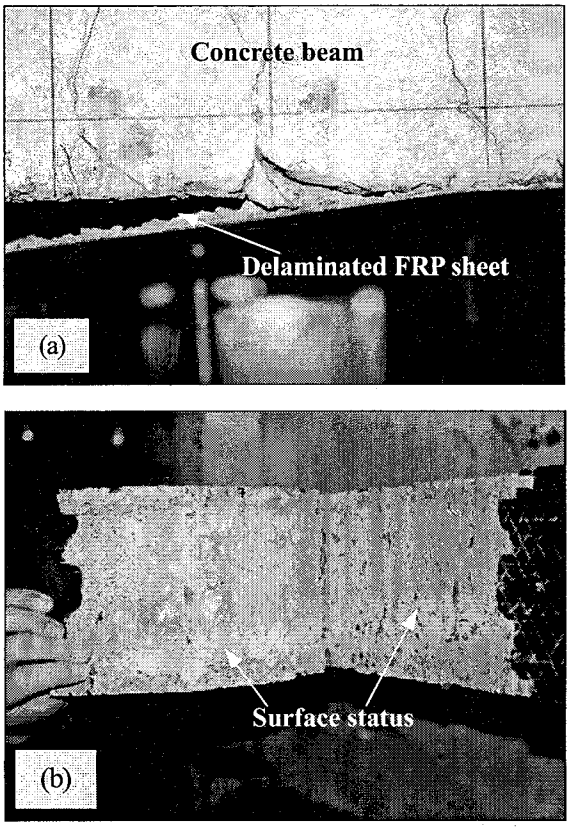

Fig. 1. Interfacial debonding fracture observed in experiments

parallel to the crack surface is also taken account by introducing shear fracture energy. Similar to smeared crack model, concrete fracture initiates in mode I, but followed by a mode II fracture along the crack surface. The simulation results are compared to that of mode II fracture assumption. It is found that both rotating and fixed smeared crack models suffer from itself limitations for shear fracture behaviors, while the displacement discontinuity model gives reasonable result. A quantitative relation of separated fracture energies G_f^I and G_f^{IIs} of concrete used in the displacement discontinuity model to G_f^{II} in mode II fracture assumption is identified.

2. Interfacial debonding behaviors

In the macroscopic viewpoint, the force transfer between FRP and concrete is achieved by adhesive resin. The debonding failure along FRP-concrete bond interface is generally modeled as mode II fracture. However, looking at the surface of delaminated FRP sheet, it is found that a layer of concrete, with thickness from 2mm to 10mm, is usually stuck on it, as presented in Fig. 1(a),(b). In addition, a finite element simulation of FRP-strengthened concrete beams by Wu and Yin[8] has also reported the interfacial debonding failure through a layer of cracked concrete elements, in form of mode I fracture(see Fig. 2). FRP strengthening can prevent flexural concrete cracks from further propagation, but the stress transfer by adhesive layer also heightens the stress level of the concrete adjacent to the bond interface. As a result, the interfacial concrete sets to crack once its tensile strength is exceeded. In this case, the crack orientation is nearly 45^0 inclined to the bond surface. With further stress transferred, more and more small interfacial concrete cracks. When these microscopic concrete cracks eventually connect through, a interfacial debonding representing macroscopic mode II fracture occurs. Different from the mode II fracture assumption, crack in concrete is considered to initiate as mode I fracture and thereafter transfers to mode II fracture with subsequent aggregate interlock along the crack surface, as shown in Fig. 3.

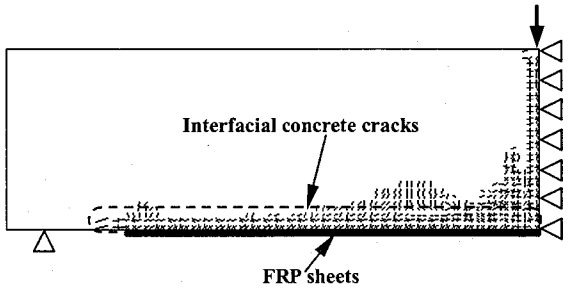

Fig. 2 Finite element simulation result of interfacial debonding in concrete

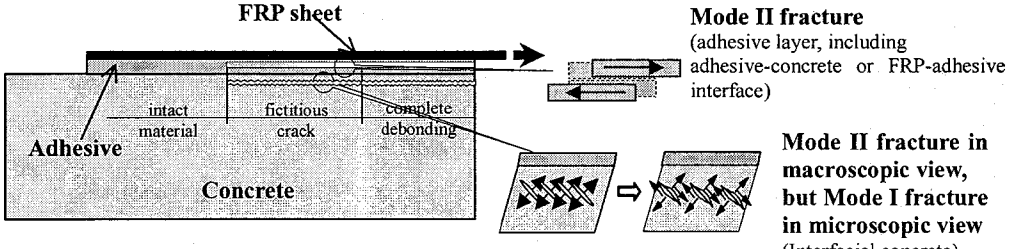

Fig. 3 Fracture mechanisms of interfacial debonding

2.1 Mode II fracture assumption(macro representation of debonding)

The interfacial debonding behavior can be expressed by a $\tau-\delta_t$ relationship. A simple linear ascending-descending $\tau-\delta_t$ relationship is usually adopted(Fig. 4), where f_b is the local bond strength, K_b is initial stiffness, and G_f^{II} is the interfacial fracture energy. All these are considered as the comprehensive properties of the bond interface.

According to the previous analytical investigations of Täljsten[1] and Wu et al.[2], the theoretical derivations are under the following assumptions: 1) adherents are homogeneous and linear elastic; 2) the adhesive resin is only exposed to shear transfer; 3) bending effect on the bond interface is not considered. The load-carrying capacity of FRP-concrete bond interface, therefore, can be approximately described in terms of interfacial fracture energy G_f^{II} , the Young's modulus E_{frp}, the width b_{FRP} and thickness t_{frp} of FRP sheets(Eq.1).

$$P_{\max} = b_{FRP}\sqrt{2E_{FRP}\,t_{FRP}\,G_f^{II}} \tag{1}$$

2.2 Mode I fracture assumption-(micro representation of debonding in concrete)

(1) Smeared Crack Models

Considering the interfacial debonding in form of concrete crack, two conventional smeared crack models are adopted[9]. One is the rotating crack model, which assumes that the crack normal continuously rotates with the changing axis of principal stress, as shown in Fig.5(a). Because the crack orientation is constantly modified, the shear interlock along the crack surface can be removed. The other is the fixed crack model, as shown in Fig.5(b), in which a constant shear retention factor β is introduced to account for the shear transfer effect like aggregate interlock. The stress-strain relationship on crack surface can be written as

$$\mathrm{D}_{cr} = \begin{bmatrix} D_n & 0 \\ 0 & D_t \end{bmatrix},$$

$$D_t = \begin{cases} (\sigma_{11}-\sigma_{22})/2(\varepsilon_{11}-\varepsilon_{22}) & \textit{rotating model} \\ \beta G & \textit{fixed model} \end{cases} \tag{2}$$

where D_n is the softening stiffness in crack normal, D_t is the stiffness along crack surface, and G is the elastic shear modulus. For rotating crack model, the shear term is implicitly calculated by rotating principal stresses and strains. In both crack models, a linear softening curve is used to describe the normal stress degradation on crack surface, as shown in Fig.6.

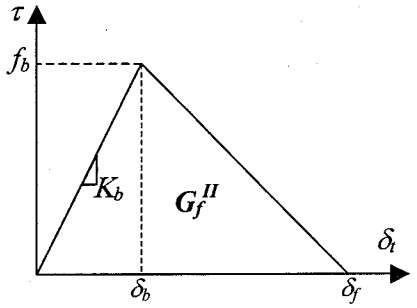

Fig. 4 Mode II fracture assumption for interfacial debonding

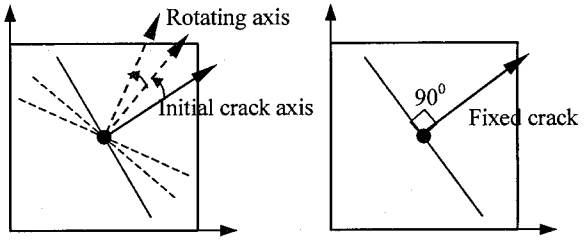

(a) Rotating crack model (b) Fixed crack model

Fig.5 Two treatments of crack discontiuities

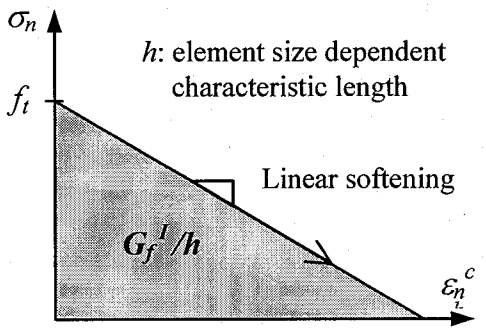

Fig. 6 Tension softening relation

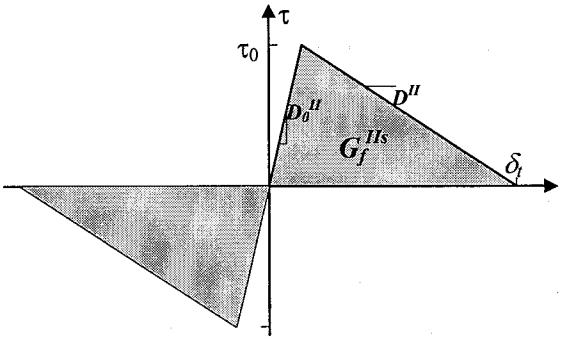

Fig. 7 Shear softening along crack surface

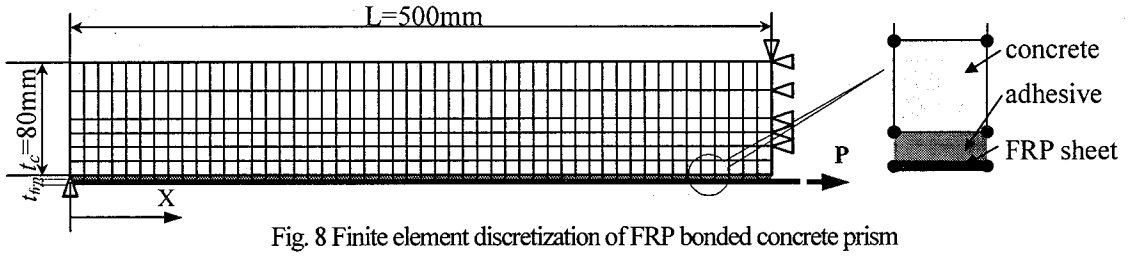

Fig. 8 Finite element discretization of FRP bonded concrete prism

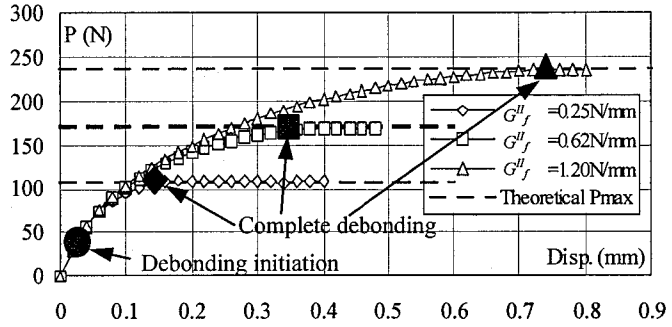

Fig. 9 load-displacement relations with varying G_f^{II} based on mode II fracture assumption

(2) Displacement Discontinuity Model

This crack model with embedded displacement discontinuity in a finite element was originally developed by Dvorkin et al.[10] for simulating the localized crack propagation in brittle materials. In the direction normal to crack, similar linear softening relation in the smeared crack models is used. The difference is that the softening model is described by a traction vs. discontinuous displacement relationship. With modification by introducing shear fracture energy G_f^{IIs}, the fracturing behavior along the crack surface could also be considered. The detailed finite element formulation can be referred to the journal paper[11].

As shown in Fig.7, D_0^{II} is the initial shear modulus when crack is triggered. It is considered to be a reduction of shear modulus G. by a multiplier α (here α=0.5). τ_0 is a pre-defined value. If the shear stress exceeds τ_0, it enters softening branch. The negative modulus D^{II} can be determined by fixing D_0^{II}, τ_0 and G_f^{IIs}

3. Finite element analysis

The interfacial debonding behavior of a concrete prism strengthened with FRP sheets is simulated. The schematic sketch and finite element mesh are presented in Fig. 8, where L is FRP sheets bond length, t_c= 80mm, and t_{FRP}= 0.1mm are the thickness of concrete prism and FRP sheets, respectively. A unit out-of-plane bond width b_c=b_{FRP}=1mm is assumed.

In the FE simulation, the concrete prism, FRP sheets and FRP-concrete bond interface are discretized by 4-node plane stress elements, truss elements and line-to-line interface elements[12] respectively. Smeared crack models or the displacement discontinuity model are to simulate the fracture in concrete. FRP sheet is kept linear elastic until rupture and debonding behavior of interface element follows the τ–δ_t relationship in previous section. Properties of each material are summarized as follows. For concrete, Young's modulus E_c=2.5×10^4 MPa, Poisson ratio ν=0.15, tensile strength is f_t=2.0MPa. For FRP sheets, Young's modulus E_{FRP}=2.3×10^{5}MPa, rupture stress of FRP sheet is 3.35×10^{3}MPa. The local bond strength of FRP-concrete interface is f_b=3.0MPa, initial stiffness is K_b=160N/mm^3, and interfacial mode II fracture energy G_f^{II}=1.2N/mm, referred to the experiment by Yoshizawa et al.[3].

3.1 Simulation based on mode II fracture assumpition

First, the interfacial debonding is assumed to propagate only within interface elements as a pure mode II fracture. To avoid the interaction of concrete crack, all the concrete element is enforced to be elastic. Varying interfacial fracture energy G_f^{II}=0.25, 0.62 and 1.2N/mm under the condition of constant local bond strength f_b=3.0Mpa and initial stiffness K_b=160N/mm^3, the load-displacement relations are obtained, as shown in Fig. 9. The debonding initiation occurs when the shear stress in resin at load end increases to local bond strength. Thereafter, the shear stress begins to decrease following the softening curve described in Fig.4 and the debonding propagate along the bond interface. When

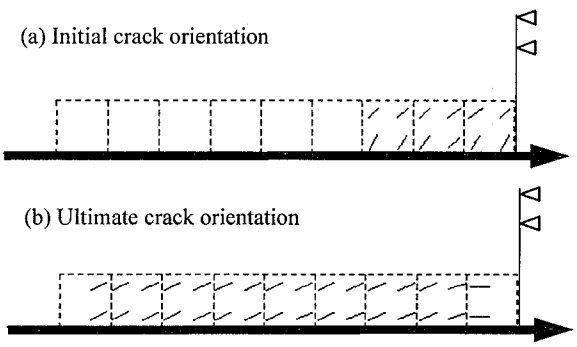

Fig. 10 Crack evolution along interfacial concrete elements

the shear stress in resin at the load end drops to zero , the maximum load-carrying capacity of bond interface is reached, after which it will be kept constant until the debonding propagates to the other FRP bond end. The load-carrying capacity of FRP-concrete bond interface are 109N, 170N and 237N, respectively. Compared to the theoretical solutions calculated by Eq.(1), it is seen that the ultimate load-carrying capacity of simulation results are exactly matched.

This implies that mode II fracture assumption can basically describe the debonding behaviors along FRP-concrete interface in a macroscopic point of view. It also provides quantitative relation between load-carrying capacity of FRP-concrete bond interface and G_f^{II} and FRP sheet properties and thickness.

3.2 Simulation based on mode I fracture assumption

For the debonding propagation through interfacial concrete, concrete crack is initiated as mode I fracture. In this case, the debonding only occurs in a thin layer of interfacial concrete while the adhesive layer is assumed perfect. Hence, the interface elements and the concrete

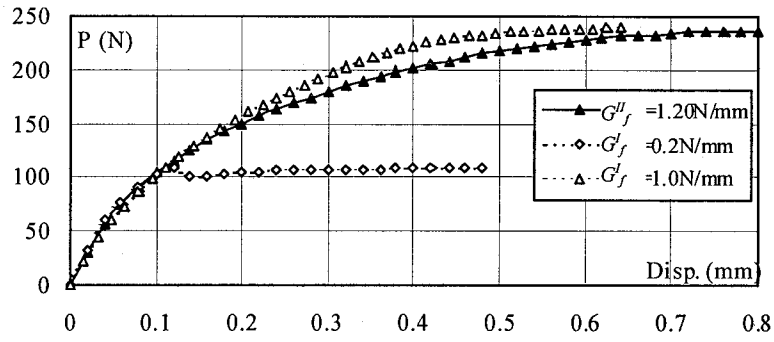

Fig. 11 Fracture energy release of mode I and mode II fracture assumption

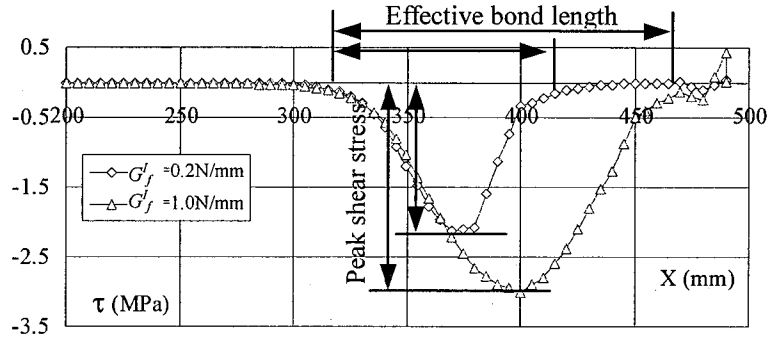

Fig. 12 Shear stress distribution of interface elements along FRP-concrete interface by rotating smeared crack model

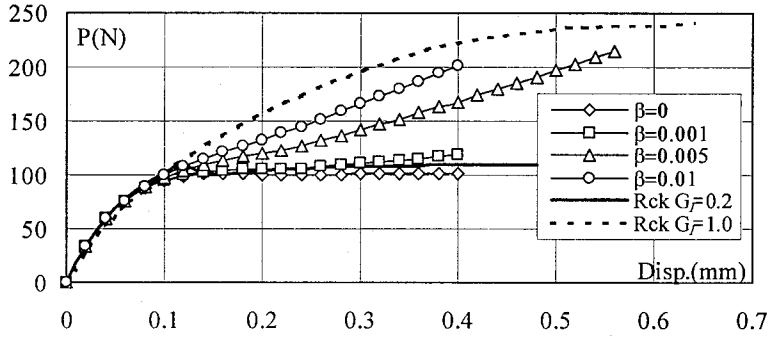

Fig. 13 Load-displacement curves with different shear retention factor β

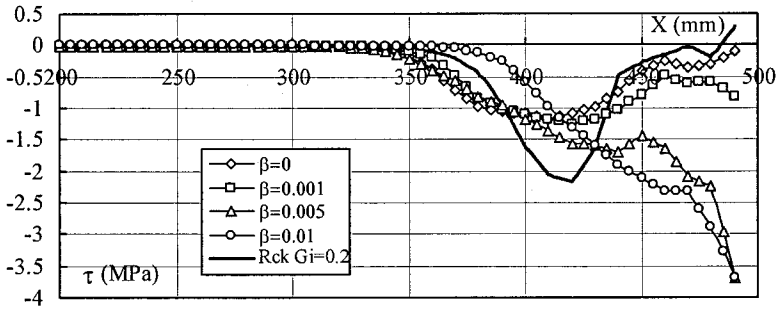

Fig. 14 Shear stress distribution of interface elements along FRP-concrete interface by fixed smeared crack model

elements except one layer bonded on the interface are enforced to be linear elastic, as shown in Fig. 8.

(1) Rotating smeared crack model

By using the rotating smeared crack model, the evolution of crack orientations at each cracked element is presented in Fig. 10. Interfacial concrete cracks initiate in the direction of nearly 45^0 or more inclined to the loading axis. With continuing load, the crack orientations gradually rotate and ultimately approach to the horizontal direction. It means that fracture starts in tension and subsequently proceeds in tension-shear. Such a simulation result implies that the rotating crack model is applicable to explain the evolution of interfacial concrete crack that finally results in the debonding failure.

With G_f^I=0.2, and 1.0N/mm, Fig.11 gives the load-displacement relationship by rotating crack model and comparison to the mode II fracture assumption with G_f^{II}=1.2N/mm. Qualitatively similar to the results obtained by mode II fracture model, the load-carrying capacity of bond interface is enhanced and eventually approaches to a constant value with the increasing mode I fracture of concrete G_f^I. Fig.12 shows the shear stress distribution of interface elements along FRP-concrete interface, which implies that the maximum shear stress and the effective bond length are enhanced by increasing fracture energy G_f^I. However, discrepancy appears when concerning the rationality of the value of mode I fracture energy for concrete. Normally, the mode I fracture energy of concrete G_f^I is generally around 0.1~0.3N/mm, based on the experimental researches (i.e. Lenke and Gerstle[13]). According to the mode II fracture assumption, G_f^{II}=1.2N/mm is also regarded as a normal value identified from the experimental data[3]. Expectantly, the same bond load-carrying capacity should have been obtained no matter whichever interfacial fracture assumption is applied. However, result shows a big difference. For rotating crack model, G_f^I must be increased to 1.0N/mm, an unpractical value of mode I fracture energy of concrete, to obtain the same load-carrying capacity of bond, in Fig.11. It could be understood that rotating crack model neglects the aggregate interlock on crack surface, so as to underestimate load-carrying capacity of bond interface. Such an aggregate interlock behavior should not be neglected in concrete cracking, especially when concrete is subjected to shear loading like the present case. To consider the aggregate interlock on concrete crack surface, an fixed smeared crack model with a constant shear retention factor is also used.

(2) Fixed smeaed crack model

Can fixed smeared crack model obtain rationable result by treating the aggregate interlock through a constant shear retention factor β? By fixing G_f^I =0.2N/mm, and varying β=0, 0.001, 0.005, 0.01, Fig.13 shows β's influence to bond capacity, where the legend "Rck" denotes rotating crack model and "β" stands the shear retention factor in fixed crack model. When β is set to zero or a rather small value, the load-carrying capacity is low and similar to that of rotating crack model. When β increases to 0.005 and 0.01, the aggregate interlock behavior is apparent. However, the load intends to increase continuously but not approaches to a ultimate state, a stable macroscopic debonding propagation. This can also be seen from the shear stress distribution of interface elements along FRP-concrete interface in Fig.14. In the cases of β=0.005 and 0.01, the shear stress at loading end does not decrease even though the interfacial crack has begun to propagate and effective bond length increases constantly. This is not an objective fracturing behavior of interface. The aggregate interlock is overestimated due to the constant accumulation of residuel shear stress along the crack surface by a unneglectable constant shear modulus and never intends to be released. It is suggested that the shear retention factor does have its physical meaning to describe the aggregate interlock behavior. But a non-zero constant shear retention factor β tends to cause the shear stress accumulation on the crack surface, thus resulting in incorrect simulation result.

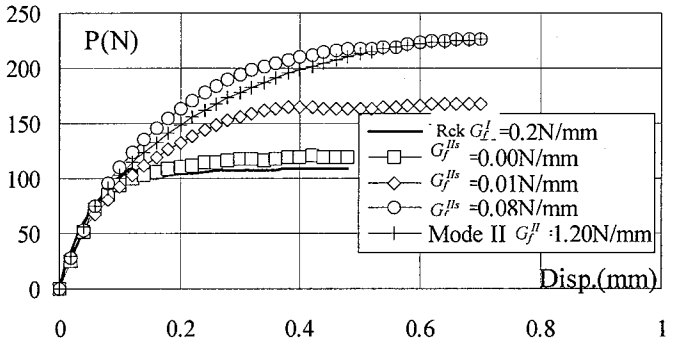

Fig. 15 Load-displacement curves with varying G_f^{IIs}

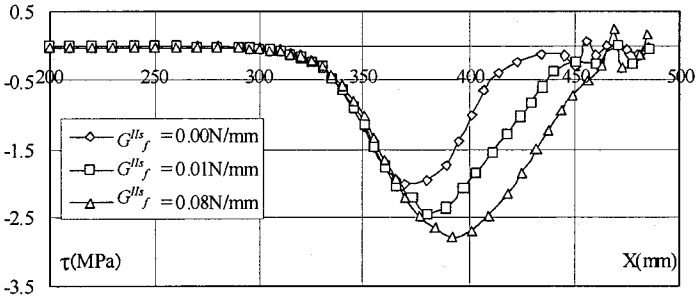

Fig. 16 Shear stress distribution in interface elements by displacement discontinuity model

(3) Displacement discontinuity model

Considering the disadvantages of both smeared crack models, a displacement discontinuity model is used, in which an embedded crack surface is formulated in an element to release the shear locking along crack surface encountered in fixed smeared crack model. Moreover a softening curve between shear stress and shear displacement is introduced for the reality by consuming shear fracture energy G_f^{IIs}. By fixing the concrete fracture energy at G_f^I=0.2N/mm as used previously and varying the shear fracture energy G_f^{IIs}, the load-carrying capacity of FRP-bonded concrete prism increases, and the ultimate value approaches a constant, as shown in Fig. 15.

By comparing to the simulation results by mode II fracture assumption and mode I fracture assumption by rotating smeared crack model, it can be seen that when G_f^{IIs} is set to zero the load-carrying capacity is on the lower limit similar to that of rotating smeared crack model, while increasing G_f^{IIs} enhances the load-carrying capacity of FRP-concrete interface. When G_f^{IIs} =0.08N/mm, the same load-carrying capacity obtained by mode II fracture assumption with G_f^{II}=1.2N/mm can be reached with unchanged mode I fracture energy G_f^I=0.2N/mm. It implies that the shear fracture energy G_f^{IIs} reflects the shear transfer ability of concrete and plays an important role when shear fracture is dominated.

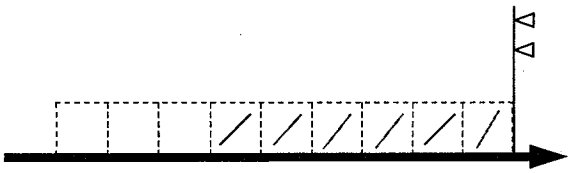

Fig. 17 Crack pattern along interfacial concrete elements by displacement discontinuity model

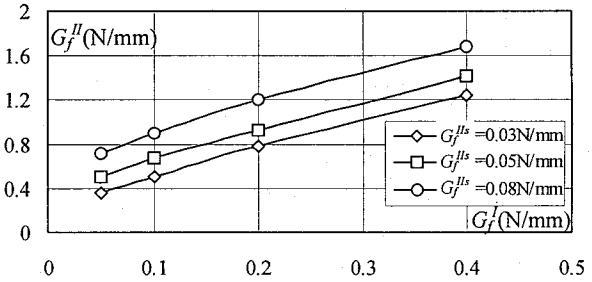

Fig. 18 G_f^I-G_f^{II} relations with varying G_f^{IIs}

The shear stress distribution of interface elements also gives reasonable results, in Fig.16. Fig.17 shows the crack pattern in interfacial concrete elements. The crack orientation in every element is fixed once it occurs, which is similar to the crack pattern by fixed smeared crack model. The difference is that displacement discontinuity model only evaluates stress state at element central point. Comparing to the fixed crack model, the unrational shear locking disappears and the effective bond length is well represented with the increase of shear fracture energy G_f^{IIs} and constant G_f^I. Through a numerical fitting by displacement

discontinuity model, a relationship between the results based on mode II fracture assumption and mode I fracture assumption in concrete followed by shear transfer is obtained and shown in Fig. 18.

In case that the debonding fracture occurs along interfacial concrete, both mode II and mode I fracture assumptions for interfacial debonding should lead to the same load-carrying capacity of the bond interface. The shear fracture energy of concrete G_f^{IIs} is regarded as a specification of both the concrete and the bonding conditions. Therefore, introducing shear fracture energy on crack surface after the mode I crack initiation bridges these two assumptions.

4. Conclusions

A finite element analysis of debonding fracture using different crack models is performed. It does not intend to discuss the goodness of one model over the others, but wants to provide a new view of the debonding mechanism more physically in the FRP-strengthened concrete structures — shear fracture in interfacial concrete. The following conclusions are drawn:

1) For the debonding fracture occurring along the interfacial concrete layer, both fracture assumptions can be adopted to evaluate the interfacial behavior. In mode II fracture assumption, the equivalent interfacial fracture energy can be correlated with some concrete properties, i.e. tensile fracture energy and shear fracture energy.
2) Rotating smeared crack model can physically describe the concrete crack evolution during debonding propagation process. But it underestimates the real aggregate interlock effect on the crack surface.
3) Fixed crack model considers the shear transfer by a constant shear retention factor β. But a big value of β may lead to accumulated residue shear stress on the crack surface that never vanishes, thus overestimating the load-carrying capacity of FRP-concrete bond.
4) In shear-dominated fracture, the fracture energy release along the crack surface plays an important role to describe the ability of shear transfer. Displacement discontinuity model that introduces shear fracture energy for shear transfer on crack surface obtains rationable results.
5) The shear fracture energy release should be bonding condition-dependent. Further study is necessary to get the quantitative relation of such a dependence, thus providing more efficient FRP reinforcing approaches.

References

1) Täljsten, B., Strengthening of concrete prisms using the plate-bonding technique, *Int. J. Frac.*, 82(3), pp.253-266, 1996
2) Wu, Z.S., Yuan, H. and Niu, H., Stress transfer and fracture propagation in different kinds of adhesive joints, *Journal of Engineering Mechanics*, ASCE, pp.562-573, 2002
3) Yoshizawa, H., Wu, Z.S., Yuan, H. and Kanakubo, T., Study on FRP-concrete interface bond performance, *Journal of Material, Concrete Structures and Pavements*, JSCE, 49(662), pp.105-119, 2000
4) Wu, Z.S., Yuan, H., Yoshizawa, H. and Kanakubo, T., Experimental/analytical study on interfacial fracture energy and fracture propagation along FRP-concrete interface. *ACI International, Special Publication* 201, pp.133-152, 2001
5) Yin, J. and Wu, Z.S., Interface crack propagation in FRP-strengthened concrete structures using nonlinear fracture mechanics. *FRPRCS-4, ACI International SP 188*, edited by Dolan et al., pp.1035-1047, 1999
6) Wu, Z. S., Matsuzaki, T. and Tanabe, K. Interface crack propagation in FRP-strengthened concrete structures. *FRPRCS-3*, 10; (1), pp.319-326, 1997
7) Wu, Z. S., Yin, J., Ishikawa, T. and Iizuka, M., Interfacial fracturing and debonding failure modes in FRP-strengthened concrete structures, *Proc. of the Fourth Joint Canada-Japan Workshop on Comp.*, pp. 403-410, 2002
8) Wu, Z.S. and Yin, J., Fracturing behaviors of FRP-strengthened concrete structures, *Eng. Frac. Mech.*, 70(10), pp.1339-1355, 2003
9) Borst, R. de Some recent developments in computational modelling of concrete fracture, *Int. J. Fracture Mechanics*, 86, pp.5-36, 1997
10) Dvorkin, E.N., Cuitino, A.M. and Gioia, G. Finite elements with displacement interpolated embedded localization lines insensitive to mesh size and distortions, *Int. J Num. Meth. Eng.*, 30, pp.541-564, 1990
11) Wu, Z. & Yin, J. Analysis of mixed-mode brittle fractures by mixed finite element with internal displacement discontinuities, *Proc. of Conf. on Comp. Eng. and Sci.*, JSCES, 3, pp.841-844, 1998
12) DIANA-7 User's Manual Lakerveld b.v., The Hague 1998.
13) Lenke, L. R. and Gerstle, W. H. Tension test of stress versus crack opening displacement using cylindrical concrete specimens, *ACI International SP 201*, edited by Vipulanandan and Gerstle, pp.189-199, 2001

(Received: April 13, 2006)